

Quantum dot emission enhancement via coupling with an epsilon-near-zero sublayer

S. Stengel,¹ J. I. Choi,² A. B. Solanki,^{2,3} H. Ather,^{4,2} P. G. Chen,² B. M. Triplett,² M. Ozlu,² K. R. Choi,^{2,5} A. Senichev,² W. Jaffray,¹ A. S. Lagutchev,² L. Caspani,⁶ M. Clerici,⁶ L. Razzari,⁷ R. Morandotti,⁷ M. Ferrera,¹ A. Boltasseva,² and V. M. Shalaev^{2, 4, 3, 8, *}

¹*Institute for Photonics and Quantum Science, Heriot-Watt University, Edinburgh EH14 4AS, UK*

²*Birck Nanotechnology Center, Purdue University, West Lafayette, Indiana 47907, USA*

³*Elmore Family School of Engineering and Computer Engineering, Purdue University, West Lafayette, Indiana 47907, USA*

⁴*Department of Physics and Astronomy, Purdue University, West Lafayette, Indiana 47907, USA*

⁵*Research Institute for Nanoscale Science & Technology, Chungbuk National University, Cheongju, Chungbuk, 28644, Republic of Korea*

⁶*Como Lake Institute of Photonics, Department of Science and High Technology, University of Insubria, Via Valleggio 11, 22100, Como, Italy*

⁷*Institut National de la Recherche Scientifique Centre Énergie Matériaux Télécommunications (INRS-EMT), 1650 Boulevard Lionel-Boulet, Varennes, Quebec J3X 1P7, Canada*

⁸*Purdue Quantum Science and Engineering Institute (PQSEI), Purdue University, West Lafayette, Indiana 47907, USA*

(Dated: 12 December 2025)

Quantum emitters operating at telecom wavelengths are essential for the advancement of quantum technologies, particularly in the development of integrated on-chip devices for quantum computing, communication, and sensing. Coupling resonant structures to an epsilon-near-zero (ENZ) environment has been shown to enhance their optical performance by both increasing spontaneous emission rates and improving emission directionality. In this work, we comparatively study emission characteristics of colloidal PbS/CdS (core/shell) quantum dots at telecom wavelengths on different substrates, where two different sets of quantum dots emitting within and outside the epsilon-near-zero region are deposited on both glass and indium tin oxide (ITO) substrates. Our results demonstrate that coupling quantum dots to the ENZ spectral region results in a reduction of photoluminescence lifetime of 54 times, a 7.5-fold increase in saturation intensity, and a relative emission cone narrowing from 17.6° to 10.3°. These results underline the strong dependence of quantum dot emission properties on the spectral overlap with the epsilon-near-zero condition, highlighting the potential of transparent conducting oxides (TCOs), such as ITO, for integration into next-generation quantum photonic devices. Due to their CMOS compatibility, fabrication tunability, and high thermal and optical damage thresholds, these ENZ materials offer a robust platform for scalable and high-performance quantum optical systems operating within the telecom bandwidth.

I. INTRODUCTION

In recent years, the field of quantum optics has witnessed a surge in applications that were once considered technologically unfeasible. Among these, solid-state quantum emitters have emerged as versatile platforms for single-photon generation, enabling advancements in quantum sensing, secure communication, and integrated quantum photonic circuits¹. In particular, emitters operating in the telecom wavelength band are key to merging quantum functionalities with existing fiber-optic infrastructures². This has catalyzed efforts towards integrating quantum emitters with an on-chip photonic environment to control emission dynamics, device complexity, and coherence^{3,4}. PbS/CdS core-shell quantum dots (QDs) are a compelling choice for these applications, thanks to their commercial availability, size-tunable emission linewidth in the near-infrared (NIR), and compatibility with non-cryogenic operation⁵. Their spectral range spans from

850 nm to 1600 nm depending on size and ligand, with improved photostability and passivation due to the CdS shell⁶. These QDs exhibit native lifetimes on the order of 1–3 μs and maintain relatively good quantum efficiency over a wide temperature range^{5,7}. The surface chemistry of QDs can also be tuned to control radiative vs. non-radiative decay pathways⁸, and their utility has been demonstrated in diverse areas from solar energy harvesting^{9,10} to bioimaging^{11,12}. However, their integration into a photonic environment that could reshape and enhance their NIR emission properties remains an open challenge.

Recently, significant interest has surged around the so called epsilon-near-zero (ENZ) materials, for which the real part of the dielectric permittivity vanishes near the plasma frequency. In these systems the decoupling between the magnetic and the electric fields is linked to several key effects (e.g., slow light, wavelength stretching, etc.) leading to a unique behaviour in the linear and nonlinear regimes^{13–18}. Also, by placing quantum emitters in a time-modulated ENZ environment, another mechanism for controlling quantum states could be realized, allowing for the design of fully opti-

*corresponding author: shalaev@purdue.edu

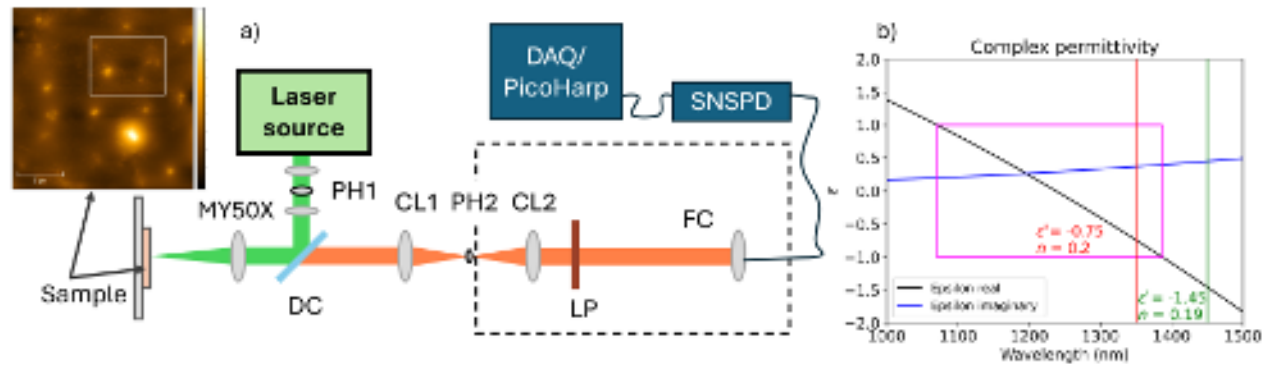


FIG. 1. Experimental setup. The figure illustrates the simplified excitation/detection scheme for both saturation and lifetime measurements. a) A laser beam centered at around 530 nm passes through a confocal pinhole (PH1), then reflects off a dichroic mirror (DC), passes through a microscope objective (MY50X), which is mounted on a 3D piezo stage, and is then focused onto the sample (Fig. 1(a) inset shows sample AFM image). The emitted signal passes the DC and is directed through PH2 (200 μm) and lenses CL1 and CL2 for spatial filtering. All components after PH2 are housed inside a blacked-out box, followed by a long-pass filter (LP) with a cut-on wavelength at 1 μm , omitting any stray light and allowing only for the emitters' signal to be detected. Further, the beam is fiber-coupled at (FC), collecting the signal and sending it to the superconducting nanowire single-photon detector (SNSPD) with high efficiency in the near-infrared. The SNSPD's electronic readout is passed to either a data acquisition device (DAQ) for counts evaluation or to the PicoHarp module for lifetime measurements. b) Dispersion curves (epsilon real, black curve, and epsilon imaginary, blue curve) of ITO. The pictures also reports the ENZ bandwidth ($|\epsilon'| < 1$ between 1070 nm and 1380 nm, pink box), and the emission lines of both QD batches at 1350 nm (red vertical line) and 1450 nm (green vertical line), as well as the real ϵ and n values for both batches.

cal quantum networks^{19,20}.

Another promising route to take advantage of ENZ systems, pertains emission engineering. For instance radiative properties of emitters in and around plasmonic or ENZ materials are strongly dependent on the materials' dimensionality, thus providing a higher degree of freedom in engineering dispersion and associated emission properties^{3,21–27}. Theoretical works also predict that coupling emitters to an ENZ environment can lead to a drastic reshaping of their radiation properties, including radiative suppression, modification of the emission directionality, and even enabling super-radiant behavior^{21,28–31}. In addition to this, the optical analogue of the Meissner effect, where ENZ substrates prevent field penetration, provides an additional degree of freedom to engineer emission directionality in a low index systems^{32,33}. Further, the manipulation of Berreman modes by altering the film thickness, in perfect absorber configuration, may allow for additional control of coupling excitation efficiency.^{18,34–40} Studies also confirm that nanoantennas placed on ENZ substrates exhibit enhanced out-of-plane radiation and narrower angular emission where the spectral overlap with the ENZ condition is met³³.

To date, a direct and broad experimental exploration of room-temperature properties of ENZ-coupled emitters within the telecom band remains limited and disjoint. In this regard it is worth mentioning a few important theoretical works pertaining emission enhancement and engineering mediated by ENZ systems at long wavelength and other experimental attainments performed on different nano-antennas coupled with ENZ environments^{30,37,41,42}. These are key results which inspire the present research.

Importantly, TCOs, close to their cross-over wavelength, are also marked by an extremely low index of refraction and

for this reason are also referred to as near-zero-index (NZI) materials. While a low refractive index is key for maximizing several nonlinear effects, the ENZ condition is more critical, when emission engineering is concerned¹⁵. For this reason in the present manuscript we will only refer to the ENZ nature of our materials. More specifically, in this work we present a comparative study of colloidal PbS/CdS QD emission properties when deposited on standard microscope glass slides and on an ITO thin films. Our analysis also considers cases where the QD emission wavelength falls within and outside the ENZ band of the ITO substrate. Within these experimental settings, we observed a 54-fold reduction in lifetime, a 7.5-fold increase in photoluminescence (PL) intensity, and a narrowing of the emission cone from 17.6° to 10.3°. These results are consistent with prior observations of radiation engineering in the ENZ environment and pave the way for scalable, CMOS-compatible platforms based on ENZ-coupling.^{8,21,28,31,33}

II. EXPERIMENTS AND DISCUSSIONS

A. Experimental setup

To investigate the emission characteristics of PbS/CdS QDs deposited on glass and ENZ ITO thin film, we employed a custom-built time-correlated single-photon counting (TCSPC) system optimized for detection in the NIR range, while simultaneously allowing for excitation in both the visible and NIR ranges. The core of the system is a confocal microscope combined with the TCSPC setup as depicted in a simplified schematic in Fig. 1(a). This setup enables the measurement of lifetime, emission directionality, and saturation behavior. Initially, the laser beam emitting around 530 nm passes through a spatial filter (PH1) to achieve the smallest possible excitation spot size. Then the beam reflects off a dichroic mirror

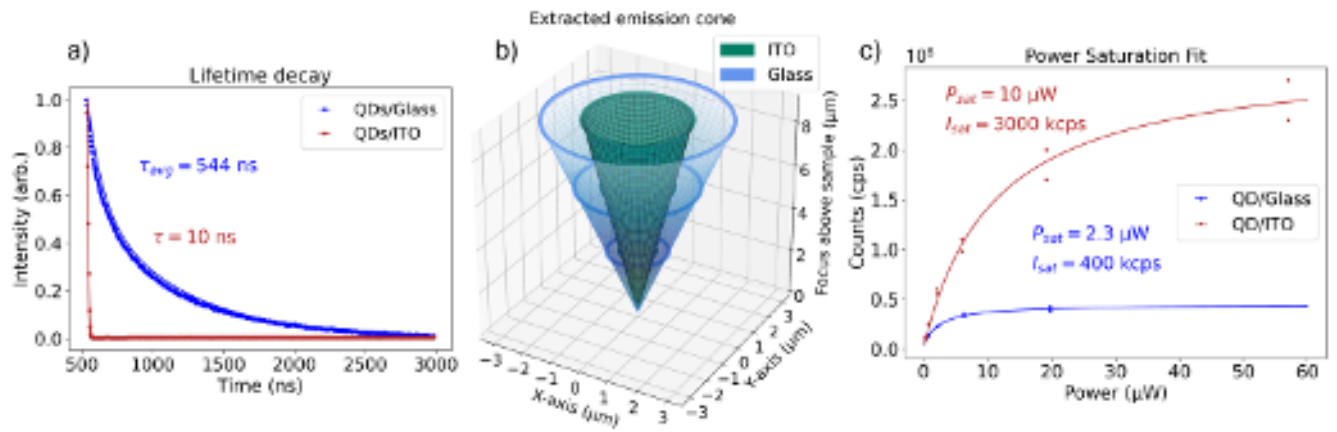


FIG. 2. Comparative analysis of QDs emitting at 1350 nm (within the ENZ bandwidth of ITO) on glass and ITO. In (a), a significant reduction of lifetime is observed, from 544 ns on glass (blue line and markers) to 10 ns when coupled to an ENZ environment (red line and markers). Panel (b) illustrates the change in directionality, with a relative emission cone narrowing from 17.6° to 10.3° for QDs on glass (blue) and on ITO (green) substrate, respectively. In (c), the saturation behavior of QDs reveals an increase in saturation power from $P_{sat} = 2.3 \mu\text{W}$ to $10 \mu\text{W}$, alongside a 7.5-fold enhancement in saturation intensity I_{sat} , from 400 kcps to 3000 kcps, when comparing QDs on ITO (red line and markers) with those on glass (blue line and markers)

(DC), with 98% reflection efficiency around the green standardized excitation wavelength, while allowing 70% transmission for the NIR emission. The excitation beam is focused onto the sample using a 0.42NA 50 \times Mitutoyo Plan Apo NIR infinity-corrected microscope objective (MY50X), resulting in a focal spot smaller than 5 μm (full-width half-maximum). This was experimentally confirmed by recording the PL images from a series of calibrated grating patterns. Confocal scanning of the sample was performed using an objective mounted on an X-Y-Z piezo stage, which allowed for nanometric positioning precision while the sample remained stationary. The emitted PL was collected through the objective and imaged onto a confocal pinhole (PH2, CL1, and CL2). All optics following PH2 are enclosed in a blacked-out box to eliminate both ambient light and residual pump, and to ensure signal collection from the focal plane only⁴³. Additionally, inside the enclosed box, a 1 μm long-pass filter was installed to ensure that only the PL from the sample was fiber-coupled and sent to the superconducting nanowire single-photon detector (SNSPD) (see Fig. 1(a)). The SNSPD output was connected to a custom-built microelectronic interface that conditioned and routed the electrical signals to either a data acquisition device (DAQ, count rate evaluation) or a PicoHarp (lifetime measurement) TCSPC module. The setup was controlled, and data was acquired via a LabVIEW code. PL maps were recorded by scanning the piezo stage with the attached microscope objective, while synchronously collecting the count rates. Subsequently, the PL maps were used to identify the most suitable regions containing spatially isolated QD ensembles. Once an emission region was identified, the microscope's objective was focused onto it to perform the lifetime measurement. For the lifetime measurements, pulses centered in the green with a full-width half-maximum duration of less than 20 ns were used to excite the QDs. We should mention that the sensitivity of our SNSPD detectors (operating at 4.2 K) is above what is required for character-

izing QD clusters (at room-temperature). Alternatively, measurements could be performed using less performant and more cost-effective equipment (e.g., SPADs). However, our experimental setup could allow for expanding the present study into the single-photon regime.

B. Sample preparation

The QDs employed in this study, sourced from CD Bioparticles, feature a commonly used PbS/CdS core/shell structure. We utilized two distinct batches of QDs, both with a mass concentration of 25 mg/ml , where one has a PL peak emission at 1350 nm, aligned with the ENZ bandwidth of the ITO sublayer, and the other one peaks at 1450 nm, which lies outside this ENZ region. To ensure optimal distribution across the substrate, the QDs were diluted in acetone at a 10:1 ratio of acetone to QDs before drop-casting. Two types of substrates were prepared to comparatively study the emission properties of the QDs. The two reference substrates were: a standard microscope glass slide, and a ~ 240 nm thick ITO thin film (associated dispersion curves are shown in Fig. 1(b)). The film thickness could be potentially used for optimizing coupling/excitation conditions; however, the choice of 240 nm thick films was solely dictated by commercial availability. Both substrate types underwent chemical cleaning, including sequential immersion in isopropanol, methanol, and acetone for 30 seconds each, including nitrogen blow-drying. Subsequently, the substrates were subjected to 90 minutes of UV-C light exposure to enhance surface wettability and promote a uniform QD dispersion. To prevent aggregation and achieve a highly uniform coating, the diluted QD solution was sonicated in an ultrasonic bath for ~ 45 minutes just prior to deposition. Following this, the solution was drop-cast onto the cleaned substrates and placed in vacuum storage boxes to accelerate solvent evaporation, ensuring an even spread of QDs. An atomic-force-microscopy (AFM) image is depicted as an inset in Fig. 1(a), showing the distribution of QD ensembles

over a select $55 \mu\text{m}^2$ area. From the cluster dimensions (200–500 nm) and the nominal QD size (~ 10 nm), the estimated number of QDs per aggregate falls in the 10^3 – 10^4 range (see supplementary material for details), which is also consistent with similar reported experimental setting in literature^{44,45}.

Importantly, the ENZ bandwidth of the ITO substrates spans from 1070 nm to 1380 nm ($|\epsilon'| < 1$), overlapping with the emission band of the first QD batch, portrayed in Fig. 1(b). Conversely, the second batch, which emits at 1450 nm, is strategically positioned outside the ENZ bandwidth of the ITO thin film, allowing for a comparative study, see Fig. 1(b).

C. Results and discussion

1. Emission within the ENZ region

We first examine the emission characteristics of PbS/CdS QDs whose emission spectrum falls within the ENZ region of the ITO substrate. A pronounced reduction in PL lifetime from 544 ns to 10 ns is observed for QDs drop-cast on the ITO substrate compared to those on glass, as reported in Fig. 2(a). In this regard, we should mention that our minimum time resolution is set by the pulse duration, setting only an upper limit to the fastest measurable decay time. The lifetime on glass is calculated using a bi-exponential fit and is averaged using an intensity-weighted formulism, according to the following equations (1) and (2)⁴⁶:

$$I_{PL}(t) = Ae^{-\frac{t}{\tau_1}} + Be^{-\frac{t}{\tau_2}}, \quad (1)$$

$$\tau_{avg} = \frac{A\tau_1^2 + B\tau_2^2}{A\tau_1 + B\tau_2}, \quad (2)$$

where $I_{PL}(t)$ is the fitted PL decay, τ_{avg} is the intensity-weighted-average lifetime, A and B are the weights, and τ_1 and τ_2 are the corresponding bi-exponential decays. The lifetime of QDs on ITO is calculated using a single exponential decay mode, due to the rapid decay and the limited number of data points. It is worth mentioning that the QDs on glass exhibited a lifetime decay similar to other reported values for PbS/CdS core/shell QDs^{5,6,8}, and that coupling to the ENZ thin film reduces the lifetime by 54 times to 10 ns. At this point, we should highlight that despite the advanced control behind QD fabrication processes, their use in integrated photonics has been primarily limited by a long decay time, impeding key applications such as high-repetition-rate photons on demand. Our results directly address this critical drawback.

From the point of view of the photon directionality, emission profiles were reconstructed by collecting the PL intensity at different focal planes at 0, 3, 6, and 9 μm on and above the sample surface. This was done while maintaining a constant excitation power density over the scanning distance, with a variation of about $\pm 3\%$ on the peak intensity. The collected data were then fit with a standard Gaussian beam divergence model to extract the angular spread. This analysis resulted in the distinct radiation signatures, as illustrated in Fig. 2(b), where a relative emission cone reduction from 17.6° on glass to 10.3° on ITO is recorded. Additionally, the large number of emitters per QD-cluster (10^3 to 10^4) guarantees high angular

emission uniformity, thus removing the need for an angular-resolved emission measurement. Finally, to characterize the saturation behavior, the count rate of the QD ensemble was monitored as the pump power was gradually increased. The saturation curves were fitted using the standard three-level emitter saturation model for optical emitters^{47,48},

$$I(P) = I_{sat} \frac{P}{P + P_{sat}}. \quad (3)$$

Here, $I(P)$ [cps] is the emission intensity as a function of the excitation power P [μW], I_{sat} [cps] is the maximum achievable saturation intensity, and P_{sat} [μW] is the power at which the system saturates, which is defined on the x-axis as the point where the intensity in counts is equal to $(1/2)I_{sat}$. It is worth underlining that from its definition the saturation power is inversely proportional to the rate at which saturation is achieved. Relating plots are shown in Fig. 2(c), where, due to the ENZ coupling, the QDs on ITO perform significantly better than the ones on glass, in terms of the saturation count rate but are worse off in terms of saturation power. Specifically, these parameters were recorded to be $I_{sat} = 3000$ kcps and 400 kcps, and $P_{sat} = 10 \mu\text{W}$ and $2.3 \mu\text{W}$, for QDs on ITO and glass, respectively.

Figure 2 compares emitters on ITO, within the ENZ window, to those on glass. This investigation reports lifetime decay, saturation behaviour, and emission directionality. The photoluminescence lifetime τ , which reflects the sum of radiative and non-radiative decay channels through $\Gamma_{tot} = \Gamma_r + \Gamma_{nr} = 1/\tau$, is reduced by a factor of 54. This indicates a very large increase in the total decay rate Γ_{tot} . The saturation curves provide two complementary quantities: the saturation power P_{sat} and the saturation intensity I_{sat} . While the former is inversely proportional to the external quantum yield $\eta_{ext} \propto \Gamma_r/\Gamma_{tot}$, the latter scales as $I_{sat} \propto \Gamma_r^2/\Gamma_{tot}$ and is therefore sensitive to the balance between the radiative rate Γ_r and the non-radiative rate Γ_{nr} . Combining the PL lifetime ratio between QDs on ITO and glass, with the associate saturation power ratio, leads to a radiative-rate enhancement of approximately one order of magnitude for the emitters on ITO (see supplementary material for details). Given that the total decay rate increases by a factor of 54, the overall dynamics is largely dominated by the rise of non-radiative decay channels.

The measured saturation intensity increases from 400 to 3000 kcps (a factor of 7.5). It is worth emphasizing that the expected saturation-intensity ratio can be directly evaluated from the radiative and non-radiative rate changes inferred from the lifetime and saturation-power measurements. Using $I_{sat} \propto \Gamma_r^2/\Gamma_{tot}$, these rates predict an intrinsic enhancement of only ~ 2.9 . However, this value is considerably smaller than the measured ratio of 7.5. This apparent discrepancy is quantitatively resolved by the ENZ-induced directionality enhancement. In fact, the relative emission cone narrows from 17.6° to 10.3° , reducing the radiated solid angle $\Omega = 2\pi(1 - \cos\theta)$ by a factor of ~ 2.9 and thereby increasing the collection efficiency by the same factor. Once this geometrical enhancement is accounted for, the corrected saturation-intensity ratio (~ 2.5 -3) agrees with the intrinsic value expected from the rate analysis within experimental uncertainty (see detailed analy-

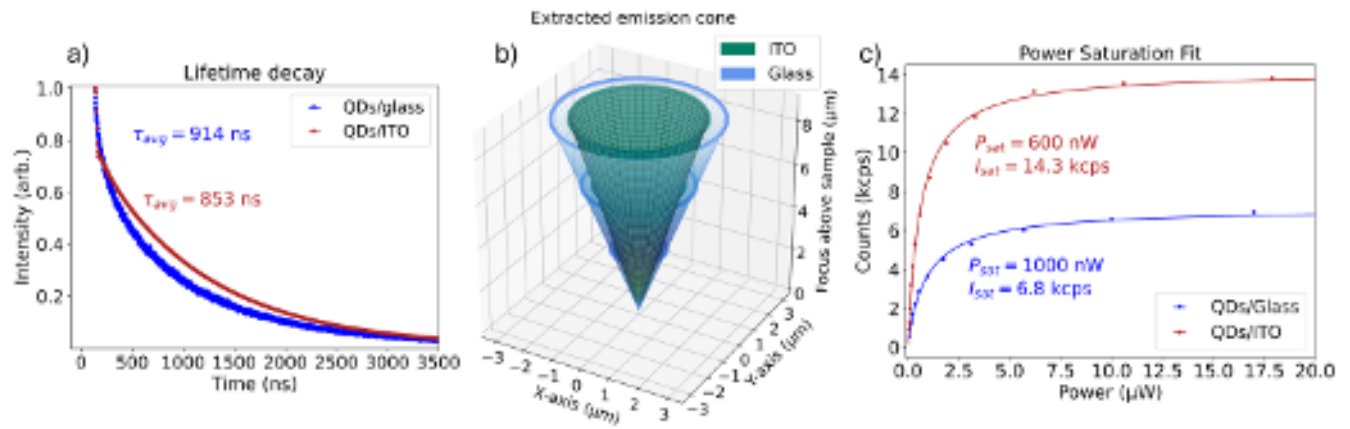


FIG. 3. Comparative analysis of QDs emitting at 1450 nm (outside the ENZ bandwidth of ITO) on glass and ITO. In (a), a minimal change of less than 10% is observed for the emitter lifetime between the cases of QDs on glass (blue line and markers) and on ITO (red line and markers), yielding 914 ns and 853 ns, respectively. Panel (b) shows the emission cones for QDs on both substrates, with a slightly narrower emission cone of 12.8° for the ITO case (green) and a wider cone of 16.0° for the QDs on glass (blue). Panel (c) depicts the saturation behavior outside the ENZ region and reveals a lower saturation power $P_{sat} = 600$ nW vs. 1000 nW, and a higher saturation intensity $I_{sat} = 14.3$ kcps vs. 6.8 kcps, when comparing QDs on ITO (red line and markers) and glass (blue line and markers), respectively.

sis on recombination channels in the supplementary material).

Overall, the ENZ sublayer leads to a drastic shortening of the PL lifetime and a reduced external quantum yield. The latter being in accordance with the typical "quenching" effect of ENZ environment. Furthermore, a strong rise of non-radiative decay, a moderate enhancement of radiative rate, and a spacial emission narrowing have been observed. All these features are consistent with ENZ-enhanced local density of optical states (LDOS), the predominance of non-radiative electromagnetic channels near the ENZ point, and the characteristic field-expulsion mechanism of ENZ interfaces^{3,30,33,41,42}.

2. Emission outside the ENZ region

In order to disentangle the emission enhancement due to the ENZ coupling from any other effect due to the presence of the ITO substrate, we performed an equivalent comparative study as the one previously reported, this time with QDs emitting at 1450 nm, outside the ENZ bandwidth. As before, measurements were focused on PL lifetime, emission directionality, and saturation behavior. For these cases, lifetimes of $\tau_{avg} = 914$ ns and $\tau_{avg} = 853$ ns have been recorded for QDs on glass and ITO, respectively. Thus, it can be seen that lifetime reduction due to the ITO substrate is still visible, but is considerably less pronounced when compared to the previous ENZ-coupled case.

The emission directionality measurements (Fig. 3(b)) show that the emission cone of QDs on ITO (green) is 12.8° , which is only slightly narrower than the 16° emission cone of QDs on glass (blue), indicating a relatively small directional enhancement.

Finally, we analyzed the power-dependent saturation behavior for QDs on both substrates, and the count rate as a function of input power (Fig. 3(c)). Here, the QDs on ITO exhibit a slightly higher saturation count rate, I_{sat} , of 14.3 kcps as com-

pared to 6.8 kcps on glass. Further, the saturation power for the QDs on ITO and glass are $P_{sat} = 600$ nW and 1000 nW, respectively. This analysis shows that the alteration in the emission properties of QDs coupled to ITO is primarily due to their emission overlap with the ENZ region. The minor effects on all investigated parameters outside of the ENZ bandwidth can be ascribed to a small plasmonic enhancement (Purcell effect). Specifically, at 1450 nm, ITO exhibits more metallic properties, thus increasing the reflectivity and contributing to the higher saturation intensity. Another factor at play is the refractive index contrast, which supports a narrower cone and therefore a more directed emission, thereby boosting the count rate at equal input power for an ITO substrate at 1450 nm compared to glass.

An additional note should be made about the QD distance from the sublayer which is expected to have an influence on the emission properties of the full cluster. This is clearly underlined by the plot in Fig.4, where the Purcell enhancement is reported as a function of the emitter-to-sublayer distance for both glass and ITO. From these curves a very strong Purcell factor enhancement and a correspondent PL lifetime reduction, is recorded for distances below 100 nm. This behaviour is also consistent with the fact that only the high-k emission components are enhanced via the ENZ regime, and they exponentially decay as the distance increase (see details in supplementary material). This plot, besides underlining the importance of the emitter distance from the ENZ surface, also provides some information about how the QDs within the same cluster see a different emission environment.

In this regard, we must underline that the size and density of QD-clusters can significantly affect their emission properties, owing to strong variations in emitter-substrate coupling, possible collective effects such as ENZ-assisted superradiance²¹, and screening phenomena in densely packed aggregates. A full reconstruction of QD-ensemble emission from the study

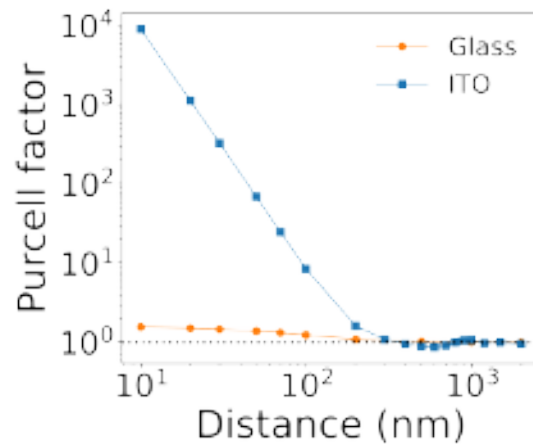


FIG. 4. Purcell factor as a function QD-to-sublayer distance for both glass and ITO cases. QDs coupled to ITO within the ENZ window (blue line with square markers) show a much stronger Purcell factor, when compared to QDs coupled to glass (orange line with dot markers), for distances below 100 nm.

of a single QD and its interactions with neighboring emitters would require a substantially broader investigation, where QD size and concentration are varied.

At this point, it is clear that the emission properties of ENZ-coupled QDs are fundamentally linked to the reconfiguration of radiative and non-radiative channels. To deepen these aspects, future studies employing sub-ps pulses of different time durations may allow for the identification of multiple recombination processes in action. Alongside these, it would be very interesting to refine our study at the single- and few-photon level. However, these investigations are outside the scope of the present phenomenological study.

III. CONCLUSION

This study presents clear experimental evidence of the profound influence that coupling to an ENZ environment can have on quantum emitter properties. When PbS/CdS (core/shell) QD emission falls within the ENZ bandwidth of the ITO-sublayer, a significant reduction in the photoluminescence lifetime from 544 ns down to 10 ns is demonstrated when compared to QDs on glass. Additionally, a 7.5-fold increase in the saturation intensity I_{sat} and a 4-fold increase in the saturation power P_{sat} were observed, suggesting a more efficient excitation-emission cycle. Furthermore, the angular emission profile narrowed significantly, from 17.6° to 10.3° , indicating a considerably improved directionality.

These enhancements are caused by the presence of the ENZ condition, as demonstrated by the comparative study performed with QD emission outside the ITO's ENZ bandwidth. Our work aims to stimulate discussions on the potential impact of low-index materials on integrated quantum technologies, motivating further studies towards single-photon emission and possible superradiant effects. The observed results clearly indicate that the ENZ environment provides a highly effective platform for controlling light-matter interactions, enabling significant improvements in emission efficiency and

directionality, all within a CMOS-compatible, telecom-band platform. Such capabilities are crucial for advancing emerging on-chip quantum optics, low-threshold quantum light sources, and tunable emitter arrays in scalable quantum photonic networks.

IV. SUPPLEMENTARY MATERIAL

The supplementary material outlines how radiative and non-radiative mechanisms together with directional effects contribute to the changes in the emitter lifetime and saturation behavior. It explains the physical origin of lifetime shortening near ENZ materials, describes how emission directionality can enhance collected intensity. Further, the supplementary material provides an estimate of the number of QDs contained within the observed QD clusters.

ACKNOWLEDGMENTS

M.F. acknowledges financial support from EPSRC project ID EP/X035158/1; AFOSR (EOARD) under award no. FA8655-23-1-7254; and EPSRC/STFC/NSERC under UK-Canada Quantum for Science Research Collaborations OPP640-APP47830. L.C. and M.C. acknowledge support from the European Commission (ERC) Consolidator Grant, QuNIm, G.A. 101125923. L.R. and R.M. are grateful for financial support from the Natural Sciences and Engineering Research Council of Canada (NSERC) through the Alliance Quantum program (Canada UK). K.C. acknowledges support by the National Research Foundation of Korea (RS-2024-00352109). Purdue co-authors acknowledge support by the US Department of Energy (DOE), Basic Energy Sciences (BES) Energy Frontier Research Center (EFRC), Quantum Photonic Integrated Design Center (QuPIDC), under the award number DE-SC0025620 (quantum emitter optical characterization); the DOE BES Division of Materials Sciences and Engineering under the award DE-SC0017717 (epsilon-near-zero materials optimization and fabrication); and Air Force Office of Scientific Research (AFOSR) under the award Number FA9550-22-1-0372 (temperature dependent characterization of quantum emitters). S.S. acknowledges META 2025 APL Quantum Best Paper Award publication fee waiver.

DATA AVAILABILITY STATEMENT

All data supporting the figures and findings presented in this manuscript are openly available under a CC BY license at [DOI: XXXXXXXX].

REFERENCES

- ¹I. Aharonovich, D. Englund, and M. Toth, "Solid-state single-photon emitters," *Nature Photonics* **10**, 631–641 (2016).
- ²S. Wehner, D. Elkouss, and R. Hanson, "Quantum internet: A vision for the road ahead," *Science* **362**, eaam9288 (2018).
- ³J.-K. So, G. H. Yuan, C. Soci, and N. I. Zheludev, "Enhancement of luminescence of quantum emitters in epsilon-near-zero waveguides," *Applied Physics Letters* **117** (2020).

This is the author's peer reviewed, accepted manuscript. However, the online version of record will be different from this version once it has been copyedited and typeset.

PLEASE CITE THIS ARTICLE AS DOI:10.1063/5.0301078

- 4J.-H. Kim, S. Aghaeimeibodi, C. J. Richardson, R. P. Leavitt, D. Englund, and E. Waks, "Hybrid integration of solid-state quantum emitters on a silicon photonic chip," *Nano Letters* **17**, 7394–7400 (2017).
- 5S. Krishnamurthy, A. Singh, Z. Hu, A. V. Blake, Y. Kim, A. Singh, E. A. Dolgoplova, D. J. Williams, A. Piryatinski, A. V. Malko, *et al.*, "Pbs/cds quantum dot room-temperature single-emitter spectroscopy reaches the telecom o and s bands via an engineered stability," *ACS Nano* **15**, 575–587 (2020).
- 6H. Zhao, H. Liang, F. Vidal, F. Rosei, A. Vomiero, and D. Ma, "Size dependence of temperature-related optical properties of pbs and pbs/cds core/shell quantum dots," *The Journal of Physical Chemistry C* **118**, 20585–20593 (2014).
- 7Y. Justo, P. Geiregat, K. Van Hoecke, F. Vanhaecke, C. De Mello Donega, and Z. Hens, "Optical properties of pbs/cds core/shell quantum dots," *The Journal of Physical Chemistry C* **117**, 20171–20177 (2013).
- 8B. Omogo, J. F. Aldana, and C. D. Heyes, "Radiative and nonradiative lifetime engineering of quantum dots in multiple solvents by surface atom stoichiometry and ligands," *The Journal of Physical Chemistry C* **117**, 2317–2327 (2013).
- 9J. J. Khanam, S. Y. Foo, Z. Yu, T. Liu, and P. Mao, "Efficient, stable, and low-cost pbs quantum dot solar cells with cr-ag electrodes," *Nanomaterials* **9**, 1205 (2019).
- 10C.-H. M. Chuang, P. R. Brown, V. Bulović, and M. G. Bawendi, "Improved performance and stability in quantum dot solar cells through band alignment engineering," *Nature Materials* **13**, 796–801 (2014).
- 11J. Q. Grim, L. Manna, and I. Moreels, "A sustainable future for photonic colloidal nanocrystals," *Chemical Society Reviews* **44**, 5897–5914 (2015).
- 12F. P. García de Arquer, D. V. Talapin, V. I. Klimov, Y. Arakawa, M. Bayer, and E. H. Sargent, "Semiconductor quantum dots: Technological progress and future challenges," *Science* **373**, eaaz8541 (2021).
- 13N. Kinsey, C. DeVault, A. Boltasseva, and V. M. Shalaev, "Near-zero-index materials for photonics," *Nature Reviews Materials* **4**, 742–760 (2019).
- 14O. Reshef, I. De Leon, M. Z. Alam, and R. W. Boyd, "Nonlinear optical effects in epsilon-near-zero media," *Nature Reviews Materials* **4**, 535–551 (2019).
- 15W. Jaffray, S. Saha, V. M. Shalaev, A. Boltasseva, and M. Ferrera, "Transparent conducting oxides: from all-dielectric plasmonics to a new paradigm in integrated photonics," *Advances in Optics and Photonics* **14**, 148–208 (2022).
- 16W. Jaffray, S. Stengel, F. Biancalana, C. B. Fruhling, M. Ozlu, M. Scalora, A. Boltasseva, V. M. Shalaev, and M. Ferrera, "Spatio-spectral optical fission in time-varying subwavelength layers," *Nature Photonics* , 1–9 (2025).
- 17J. B. Khurgin, M. Clerici, V. Bruno, L. Caspani, C. DeVault, J. Kim, A. Shaltout, A. Boltasseva, V. M. Shalaev, M. Ferrera, *et al.*, "Adiabatic frequency shifting in epsilon-near-zero materials: the role of group velocity," *Optica* **7**, 226–231 (2020).
- 18F. Bello, A. F. Page, A. Pusch, J. M. Hamm, J. F. Donegan, and O. Hess, "Combining ϵ -near-zero behavior and stopped light energy bands for ultra-low reflection and reduced dispersion of slow light," *Scientific Reports* **7**, 8702 (2017).
- 19A. Prain, S. Vezzoli, N. Westerberg, T. Roger, and D. Faccio, "Spontaneous photon production in time-dependent epsilon-near-zero materials," *Physical Review Letters* **118**, 133904 (2017).
- 20L. Vertchenko, N. Akopian, and A. V. Lavrinenko, "Epsilon-near-zero grids for on-chip quantum networks," *Scientific Reports* **9**, 6053 (2019).
- 21R. Fleury and A. Alu, "Enhanced superradiance in epsilon-near-zero plasmonic channels," *Physical Review B—Condensed Matter and Materials Physics* **87**, 201101 (2013).
- 22M. Lobet, I. Liberal, E. N. Knall, M. Z. Alam, O. Reshef, R. W. Boyd, N. Engheta, and E. Mazur, "Fundamental radiative processes in near-zero-index media of various dimensionalities," *ACS Photonics* **7**, 1965–1970 (2020).
- 23M. Y. Shalaginov, V. V. Vorobyov, J. Liu, M. Ferrera, A. V. Akimov, A. Lagutchev, A. N. Smolyaninov, V. V. Klimov, J. Irudayaraj, A. V. Kildishev, *et al.*, "Enhancement of single-photon emission from nitrogen-vacancy centers with tin(al, sc) n hyperbolic metamaterial," *Laser & Photonics Reviews* **9**, 120–127 (2015).
- 24S. Bogdanov, M. Y. Shalaginov, A. Akimov, A. S. Lagutchev, P. Kapitlanova, J. Liu, D. Woods, M. Ferrera, P. Belov, J. Irudayaraj, *et al.*, "Electron spin contrast of purcell-enhanced nitrogen-vacancy ensembles in nanodiamonds," *Physical Review B* **96**, 035146 (2017).
- 25S. Li, P. Xu, and Y. Xu, "Local photonic density of states in hyperbolic metasurfaces," *Journal of Optics* **23**, 115101 (2021).
- 26G. V. Naik, V. M. Shalaev, and A. Boltasseva, "Alternative plasmonic materials: beyond gold and silver," *Advanced Materials* **25**, 3264–3294 (2013).
- 27Y. Wang, A. Capretti, and L. Dal Negro, "Wide tuning of the optical and structural properties of alternative plasmonic materials," *Optical Materials Express* **5**, 2415–2430 (2015).
- 28O. Mello, Y. Li, S. A. Camayd-Muñoz, C. DeVault, M. Lobet, H. Tang, M. Lonçar, and E. Mazur, "Extended many-body superradiance in diamond epsilon-near-zero metamaterials," *Applied Physics Letters* **120** (2022).
- 29K.-R. Choi, M. Kim, J. W. Wu, A. D'aléo, and Y. U. Lee, "Directive emission from polymeric fluorophore with epsilon-near-zero squaraine molecular film," *Nanophotonics* **12**, 2471–2478 (2023).
- 30T. Gong, I. Liberal, M. Camacho, B. Spreng, N. Engheta, and J. N. Munday, "Radiative energy band gap of nanostructures coupled with quantum emitters around the epsilon-near-zero frequency," *Physical Review B* **106**, 085422 (2022).
- 31A. Sivan and M. Orenstein, "Enhanced superradiance of quantum sources near nanoscaled media," *Physical Review B* **99**, 115436 (2019).
- 32F. J. Rodríguez-Fortuño, A. Vakil, and N. Engheta, "Electric levitation using ϵ -near-zero metamaterials," *Physical Review Letters* **112**, 033902 (2014).
- 33J. Kim, A. Dutta, G. V. Naik, A. J. Giles, F. J. Bezares, C. T. Ellis, J. G. Tischler, A. M. Mahmoud, H. Caglayan, O. J. Glembocki, *et al.*, "Role of epsilon-near-zero substrates in the optical response of plasmonic antennas," *Optica* **3**, 339–346 (2016).
- 34W. D. Newman, C. L. Cortes, J. Atkinson, S. Pramanik, R. G. DeCorby, and Z. Jacob, "Ferrell–berreman modes in plasmonic epsilon-near-zero media," *Acs Photonics* **2**, 2–7 (2015).
- 35S. Vassant, J.-P. Hugonin, F. Marquier, and J.-J. Greffet, "Berreman mode and epsilon near zero mode," *Optics Express* **20**, 23971–23977 (2012).
- 36B. Harbecke, B. Heinz, and P. Grosse, "Optical properties of thin films and the berreman effect," *Applied Physics A* **38**, 263–267 (1985).
- 37J. Yoon, M. Zhou, M. A. Badsha, T. Y. Kim, Y. C. Jun, and C. K. Hwangbo, "Broadband epsilon-near-zero perfect absorption in the near-infrared," *Scientific Reports* **5**, 12788 (2015).
- 38T. S. Luk, S. Campione, I. Kim, S. Feng, Y. C. Jun, S. Liu, J. B. Wright, I. Brener, P. B. Catrysse, S. Fan, *et al.*, "Directional perfect absorption using deep subwavelength low-permittivity films," *Physical Review B* **90**, 085411 (2014).
- 39B.-Z. Dong, G.-J. Fang, J.-F. Wang, W.-J. Guan, and X.-Z. Zhao, "Effect of thickness on structural, electrical, and optical properties of znO: Al films deposited by pulsed laser deposition," *Journal of Applied Physics* **101** (2007).
- 40S. Saha, M. G. Ozlu, S. N. Chowdhury, B. T. Diroll, R. D. Schaller, A. Kildishev, A. Boltasseva, and V. M. Shalaev, "Tailoring the thickness-dependent optical properties of conducting nitrides and oxides for epsilon-near-zero-enhanced photonic applications," *Advanced Materials* **35**, 2109546 (2023).
- 41I. Liberal and N. Engheta, "Nonradiating and radiating modes excited by quantum emitters in open epsilon-near-zero cavities," *Science Advances* **2**, e1600987 (2016).
- 42E. Minerbi, S. Sideris, J. B. Khurgin, and T. Ellenbogen, "The role of epsilon near zero and hot electrons in enhanced dynamic thz emission from nonlinear metasurfaces," *Nano Letters* **22**, 6194–6199 (2022).
- 43M. Minsky, "Memoir on inventing the confocal scanning microscope," *Scanning* **10**, 128–138 (1988).
- 44M. A. Boles, M. Engel, and D. V. Talapin, "Self-assembly of colloidal nanocrystals: from intricate structures to functional materials," *Chemical Reviews* **116**, 11220–11289 (2016).
- 45M. P. Boneschanscher, W. H. Evers, J. J. Geuchies, T. Altantzis, B. Goris, F. T. Rabouw, S. Van Rossum, H. S. van der Zant, L. D. Siebbeles, G. Van Tendeloo, *et al.*, "Long-range orientation and atomic attachment of nanocrystals in 2d honeycomb superlattices," *Science* **344**, 1377–1380 (2014).
- 46Y. Li, S. Natakorn, Y. Chen, M. Safar, M. Cunningham, J. Tian, and D. D.-U. Li, "Investigations on average fluorescence lifetimes for visualizing multi-exponential decays," *Frontiers in Physics* **8**, 576862 (2020).
- 47S. I. Bogdanov, M. Y. Shalaginov, A. S. Lagutchev, C.-C. Chiang, D. Shah, A. S. Baburin, I. A. Ryzhikov, I. A. Rodionov, A. V. Kildishev, A. Boltasseva, *et al.*

seva, *et al.*, “Ultrabright room-temperature sub-nanosecond emission from single nitrogen-vacancy centers coupled to nanopatch antennas,” *Nano Letters* **18**, 4837–4844 (2018).

⁴⁸X. Xu, A. B. Solanki, D. Sychev, X. Gao, S. Peana, A. S. Baburin, K. Pagadala, Z. O. Martin, S. N. Chowdhury, Y. P. Chen, *et al.*, “Greatly enhanced emission from spin defects in hexagonal boron nitride enabled by a low-loss plasmonic nanocavity,” *Nano Letters* **23**, 25–33 (2022).

This is the author's peer reviewed, accepted manuscript. However, the online version of record will be different from this version once it has been copyedited and typeset.

PLEASE CITE THIS ARTICLE AS DOI:10.1063/5.0301078